The Journal of Chemical Physics

RESEARCH ARTICLE | MAY 31 2024

Interfacial host–guest complexation for inverted perovskite solar cells

Special Collection: 2024 JCP Emerging Investigators Special Collection

Kevin Ballestas ; Jovana V. Milić ; Daniel Ramírez

Check for updates

J. Chem. Phys. 160, 204712 (2024)
https://doi.org/10.1063/5.0202163

View Online
Export Citation

Articles You May Be Interested In

Energy conversion and transport in molecular-scale junctions

Appl. Phys. Rev. (October 2024)

23 May 2025 19:30:30



The Journal of Chemical Physics
Special Topics Open for Submissions
Learn More
AIP Publishing

AIP Publishing

The Journal of Chemical Physics ARTICLE pubs.aip.org/aip/jcp

Interfacial host–guest complexation for inverted perovskite solar cells

Cite as: J. Chem. Phys. 160, 204712 (2024); doi: 10.1063/5.0202163
Submitted: 2 February 2024 • Accepted: 6 May 2024 •
Published Online: 31 May 2024

View Online Export Citation CrossMark

Kevin Ballestas,[1] Jovana V. Milić,[2,a)] and Daniel Ramírez[1,a)]

AFFILIATIONS

[1] Centro de Investigación, Innovación y Desarrollo de Materiales (CIDEMAT), Faculty of Engineering, Universidad de Antioquia, Calle 70 #52-21, Medellín, Colombia
[2] Adolphe Merkle Institute, University of Fribourg, CH-1700 Fribourg, Switzerland

Note: This paper is part of the 2024 JCP Emerging Investigators Special Collection.
[a)] **Authors to whom correspondence should be addressed:** jovana.milic@unifr.ch and estiben.ramirez@udea.edu.co

ABSTRACT

Perovskite solar cells have demonstrated exceptional development over the past decade, but their stability remains a challenge toward the application of this technology. Several strategies have been used to address this, and the use of host–guest complexation has recently attracted more interest. However, this approach has primarily been exploited in conventional perovskite solar cells based on n-i-p architectures, while its use in inverted p-i-n devices remains unexplored. Herein, we employ representative crown ether, dibenzo-24-crown-8, for interfacial host–guest complexation in inverted perovskite solar cells based on methylammonium and methylammonium-free formamidinium-cesium halide perovskite compositions. Upon post-treatment of the perovskite films, we observed nanostructures on the surface that were associated with the reduced amount of trap states at the interface with the electron transport layer. As a result, we demonstrate improved efficiencies and operational stabilities following ISOS-D-2I and ISOS-L-2I protocols, demonstrating the viability of this approach to advance device stability.

© 2024 Author(s). All article content, except where otherwise noted, is licensed under a Creative Commons Attribution-NonCommercial-NoDerivs 4.0 International (CC BY-NC-ND) license (https://creativecommons.org/licenses/by-nc-nd/4.0/). https://doi.org/10.1063/5.0202163

23 May 2025 19:30:30

I. INTRODUCTION

Hybrid perovskite materials have attracted immense interest in the fabrication of solar cells, showing an unprecedented increase in their efficiency from 3.8% to over 26% in a decade.[1] This development is attributed to the superior optoelectronic properties of this material, displaying high absorption coefficients, long carrier lifetimes, and tunable bandgaps.[2–4] These properties make them suitable for applications in photovoltaics, including flexible solar devices, tandem solar cells, and light-emitting diodes.[5–7] Initially, the most widely used hybrid perovskite material for the fabrication of perovskite solar cells (PSCs) was archetypal methylammonium (MA)-based $MAPbI_3$ perovskite, which had been previously employed in dye-sensitized solar cells.[8] Since its introduction in 2014,[9] MA-free formamidinium (FA)-based perovskite materials gained increasing relevance in the field due to better thermal stability and narrower bandgaps, which are advantageous for enhancing the performance and lifetime of solar cell devices.[9,10] Consequently, the most efficient devices are currently fabricated using FA-based perovskites as light absorbers.[11] Despite these advancements, there are still challenges associated with these materials and their stability.[12,13] In particular, PSCs degrade rapidly when exposed to extrinsic stressors, such as temperature and humidity, and device architectures, i.e., regular (n-i-p) or inverted (p-i-n), play a role in the stability. It has been established that regular device structures typically yield better performances, while inverted devices offer more reliable operation stability, reduced hysteresis, and lower-temperature fabrication processes, which is beneficial for up-scaling,[14] with efficiencies over 25%.[15] To improve the intrinsic instability of the hybrid perovskite materials that are associated with ion migration processes during operation, several strategies have been used, including bulk and interfacial passivation as well as solvent, additive, and compositional engineering.[16–18] Among these strategies, applications of host–guest complexation have been especially relevant, taking advantage of the ion-binding capabilities of host molecules.[19–22] Accordingly, the use of host molecules, such as crown ethers,

© Author(s) 2024

has recently gained attention in perovskite photovoltaics.[23] Crown ethers have been used to control the solubility of materials in precursor solutions,[24] improve the uniformity during crystal growth of hybrid perovskite layers,[25] passivate surface and intergranular defects in the perovskite material,[24] address stability issues related to the migration of lithium cations,[26] and passivate buried interfaces for improving efficiency and stability of PSCs.[27] Furthermore, in contrast to other methodologies that rely on vacuum deposition,[28,29] the solution processing makes the approach compatible with high-throughput manufacturing processes, namely, slot-die coating and roll-to-roll-oriented printing. This is particularly beneficial for scaling up in the context of the commercialization of perovskite photovoltaics, which is one of the key challenges in the research field.[30–32] Nonetheless, the application of host–guest complexation via crown ethers has mostly been explored in devices with conventional n-i-p structures, and only recently, attention has been driven toward their use in inverted p-i-n architectures. At the time of preparing this report, a recent study showed that in inverted $MAPbI_3$ PSCs, the careful selection of functionalized crown ether molecules employed as dopants in the precursor solution allows for a more homogeneous film formation.[33] This approach, however, remains underexploited for alternative compositions in inverted PSCs.

In this work, the host–guest complexation strategy is applied for interfacial modulation in inverted PSCs using both MA-based and MA-free perovskite materials as light absorbers. For this purpose, a crown ether solution based on dibenzo-24-crown-8 (DB24C8) was employed as a treatment on the surface of $MAPbI_3$ and $Cs_{0.1}FA_{0.9}PbI_{2.55}Br_{0.45}$ perovskite films (Fig. 1). This treatment led to the formation of nanostructures at the perovskite/phenyl-C_{61}-butyric acid methyl ester ($PC_{61}BM$) interface displaying host–guest interactions with the perovskite cation, which were identified via attenuated total reflectance-Fourier transform infrared (ATR-FTIR) spectroscopy. Consequently, a reduction in the amount of trap states at the perovskite/$PC_{61}BM$ interface was achieved across perovskite compositions, as revealed by surface photovoltage (SPV) and photoluminescence (PL) measurements. This was found to be dependent on the amount of DB24C8 employed since it influences the nature of the trap states and excessive DB24C8 results in further trap states appearing. As a result, ISOS-D-2I and ISOS-L-2I stability tests for over 500 h[34] demonstrated that this approach is suitable for improving the operational stability of MA-based and MA-free devices without compromising their performance.

II. EXPERIMENTAL

A. Materials

Type II deionized water, lead (II) iodide (PbI_2, 99.99%), cesium iodide (CsI, >99%), and lead bromide ($PbBr_2$, >98%) from TCI; methylammonium iodide (MAI, >99.9%), methylammonium chloride (MACl, >99.99%), and formamidinium iodide (FAI, >99.99%) from Greatcell Solar Materials; dibenzo-24-crown-8 (DB24C8, 98%) from abcr; phenyl-C_{61}-butyric acid methyl ester ($PC_{61}BM$) and rhodamine 101 from 1-material, silver pellets from inMaterials, indium tin oxide (ITO) coated glass substrates from Naranjo; nickel oxide (NiO_x) nanoparticles prepared as shown elsewhere;[35] deuterated chloroform ($CDCl_3$, 99.5%) from Eurisotope; deuterated toluene (toluene-d_8, >99.95%) from Apollo Scientific; 33 wt. % methylamine solution in absolute ethanol (denatured with 1% toluene), acetonitrile (ACN, anhydrous, 99.8%), ethanol (anhydrous, >99.5%), chlorobenzene (CB, anhydrous, 99.8%), dimethyl sulfoxide (DMSO, anhydrous, >99.9%), and anisole (99%) from Sigma-Aldrich; and *N*,*N*-dimethylformamide (DMF, anhydrous, 99.8%) from Alfa Aesar.

B. Precursor solutions

NiO_x *precursor solution* was prepared by dissolving NiO_x nanoparticles in deionized water (23 mg/ml). The solution was ultrasonicated for 20 min and filtered with a 0.45 μm polytetrafluoroethylene (PTFE) hydrophobic filter before use.

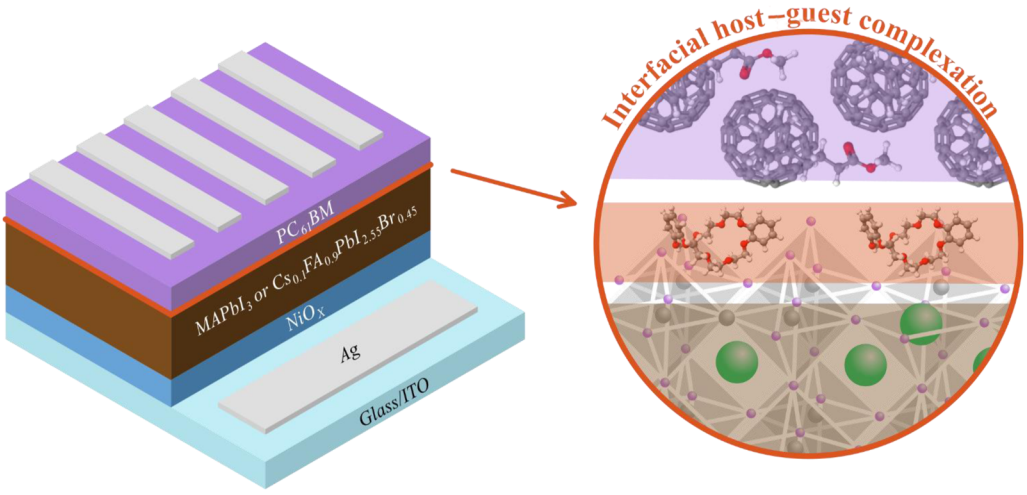

FIG. 1. Schematic representation of the device architecture and host–guest complexation treatment addressed in this study. The depicted crown ether molecule is DB24C8.

23 May 2025 19:30:30

© Author(s) 2024

$MAPbI_3$ *perovskite precursor* was prepared by dissolving pre-synthesized $MAPbI_3$ powder and MACl (1 mg of MACl per 300 mg of perovskite powder) in methylamine solution (4 mol of methylamine per mol of perovskite). The solution was further dissolved in ACN until a concentration of 30 wt. % (perovskite powder with respect to the total weight of the solution) was reached. Finally, the solution was filtered using a 0.45 μm PTFE filter. The solution was used 1 day after preparation.

$Cs_{0.1}FA_{0.9}PbI_{2.55}Br_{0.45}$ *perovskite precursor solutions* were prepared by mixing several precursor solutions in appropriate amounts. PbI_2 solution was prepared by dissolving PbI_2 in DMF:DMSO (4:1 volume/volume ratio) to a concentration of 1.85M. $PbBr_2$ solution was prepared by dissolving $PbBr_2$ in DMF:DMSO (4:1 volume/volume ratio) to a concentration of 1.5M. CsI solution was prepared by dissolving CsI in DMSO to a concentration of 1.5M. The real concentration of the solutions was calculated by measuring their density.[36] Subsequently, FAI was dissolved using appropriate amounts of the previous solutions and DMF:DMSO (4:1 volume/volume ratio) until a 1.35M concentration of $Cs_{0.1}FA_{0.9}PbI_{2.55}Br_{0.45}$ was reached. For example, to prepare 933 μl (1.35M) of $Cs_{0.1}FA_{0.9}PbI_{2.55}Br_{0.45}$ perovskite precursor solution, 195 mg of FAI were dissolved using 616 μl of PbI_2 solution (real concentration = 1.585M), 199 μl of $PbBr_2$ solution (real concentration = 1.426M), 87 μl of CsI solution (real concentration = 1.440M), and 31 μl of DMF: DMSO (4:1 volume/volume ratio).

DB24C8 *solutions* were prepared by dissolving DB24C8 in CB until the desired concentration was reached. Afterward, the solutions were filtered using a 0.45 μm PTFE hydrophobic filter.

$PC_{61}BM$ *solution* was prepared by dissolving $PC_{61}BM$ in CB (16 mg/ml). The solution was prepared the same day of use, and before deposition, it was left under constant stirring with a magnetic bar at 65 °C.

For treating the $PC_{61}BM$ *precursor solution with* DB24C8, a separate concentrated solution of DB24C8 was prepared by dissolving it in CB (30 mM). The $PC_{61}BM$ precursor solution and the concentrated DB24C8 solution were then mixed until a DB24C8 concentration of 1 mM was reached. For example, 401 μl of $PC_{61}BM$ precursor solution (16 mg/ml) were mixed with 14 μl of DB24C8 concentrated solution (30 mM) to reach a 1 mM concentration of DB24C8 in the final solution.

Rhodamine 101 *solution* was prepared by dissolving rhodamine 101 in ethanol (0.5 mg/ml). The solution was filtered using a 0.45 μm PTFE hydrophilic filter before use.

C. Fabrication of inverted perovskite solar cells and thin films

Devices were fabricated on patterned ITO-coated glass. The substrates were washed with neutral soap and sequentially sonicated with deionized water, acetone, and isopropanol for 15 min each. Then, ultraviolet ozone treatment was performed for 15 min. Immediately after, the hole transporting layer was prepared, for which 80 μl of NiO_x precursor solution was statically spin-coated on top of the ITO-coated glass at 3000 and 1000 rpm/s for 30 s. The substrates were then moved to a dry box at a relative humidity of 15%, and perovskite precursor solution was deposited on top of the NiO_x layer.

For MA-based inverted PSCs, 50 μl of $MAPbI_3$ precursor solution were dynamically spin-coated at 4000 and 4000 rpm/s for 30 s. After this, when needed, the perovskite films were post-treated using the corresponding solution (DB24C8 in CB with different concentrations detailed in the manuscript), which was dynamically spin-coated using the same conditions as the perovskite precursor. After this, the device was annealed at 100 °C for 10 min, and $PC_{61}BM$ solution (or $PC_{61}BM$ with DB24C8) was dynamically spin-coated at 2000 and 2000 rpm/s for 30 s, after which the devices were annealed at 70 °C for 5 min. After that, 50 μl of rhodamine 101 solution was dynamically spin-coated at 4000 and 4000 rpm/s for 30 s. Finally, the device was patterned using a laser-scribing process, and silver was deposited as an electrode (with a thickness of ~100 nm) via thermal evaporation.

For MA-free inverted PSCs, 60 μl of perovskite precursor solution was statically spin-coated at 4500 and 900 rpm/s for 40 s. 150 μl of anisole were dropped as the antisolvent 5 s before the end of the spin-coating process. The film was annealed at 120 °C for 30 min. When post-treatment was employed, DB24C8 precursor solution was dynamically spin-coated on top of the perovskite film at 4000 and 4000 rpm/s for 30 s, and the device was subjected to further annealing at 100 °C for 5 min. Following this, $PC_{61}BM$ (or $PC_{61}BM$ doped with DB24C8) was dynamically spin-coated at 2000 and 2000 rpm/s for 30 s, after which the devices were annealed at 70 °C for 5 min. Finally, the device was patterned using a laser-scribing process, and silver was deposited as an electrode (with a thickness of ~100 nm) via thermal evaporation.

D. Characterization

Current density–voltage measurements were performed using a 4200SCS Keithley system at a voltage sweep speed of around 100 mV/s in combination with an Oriel Sol3A solar simulator calibrated to AM 1.5G conditions.

Atomic force microscopy (AFM), surface photovoltage (SPV), and Kelvin probe force microscopy (KPFM) measurements were performed using MFP-3D equipment. For AFM, a soft silicon tip with a nominal spring constant of 2 N/m and resonance frequency of 70 kHz was used (AC240TS-R3). For KPFM, a soft silicon tip with a titanium/iridium coating, a nominal spring constant of 2.8 N/m, and a resonance frequency of 75 kHz was used (ASYELEC.01-R2). For SPV, the KPFM measurements were carried out using the dual-pass technique[37] on samples under different illumination conditions: 0% (dark), 30%, 60%, and 100% of the illumination power of a white LED. Each sample was measured under all the illumination conditions, and each measurement was performed three times, from which the corresponding error bars were calculated. SPV was plotted against the percentage of illumination as described elsewhere.[38]

UV–vis spectrometry measurements were performed on a Cary 100 spectrophotometer from Varian Inc. *Steady-state photoluminescence (PL) measurements* were performed on a Cary Eclipse fluorescence spectrophotometer from Varian Inc.

X-ray diffraction (XRD) measurements were performed on a Rigaku MiniFlex 600 diffractometer. The samples were scanned from $2\theta = 2°–60°$ using Cu ($\lambda = 1.5405$ Å) radiation, the voltage was 40 kV and the current 15 mA.

23 May 2025 19:30:30

© Author(s) 2024

Attenuated total reflectance-Fourier transform infrared (ATR-FTIR) spectroscopy measurements were performed on a Nicolet iS50 FTIR spectrometer from ThermoScientific.

Proton nuclear magnetic resonance (^{1}H-NMR) measurements were performed on a 500 MHz Bruker Ascend NMR magnet, which was controlled with an Avance III HD console and equipped with a 24-position SampeCase autosampler.

III. RESULTS AND DISCUSSION

A. Host–guest complexation in inverted perovskite solar cells

DB24C8 was employed to modulate the perovskite/$PC_{61}BM$ interface in both MA-based and MA-free inverted PSCs based on their geometric compatibility with both A cations and the ability to bind uncoordinated Pb^{2+} cations on the perovskite surface, which can contribute to the passivation of the interface and improve its stability.[24,39] In the first case, archetypal $MAPbI_3$ was employed as a light absorber, whereas MA-free perovskite with a composition of $Cs_{0.1}FA_{0.9}PbI_{2.55}Br_{0.45}$ was used for comparison. Both were studied in ITO/NiO_x/perovskite/$PC_{61}BM$/Ag p-i-n perovskite solar cell architecture. The crown ether modulation was performed at the interface with the electron-transport layer (Fig. 1), in accordance with the procedure detailed in the Experimental section. This was based on the assumption that the crown ether host would facilitate the interaction with the fullerene-based acceptor,[22,40,41] thereby improving the contact between the perovskite and the charge-transfer layer that is relevant to the stabilities and performances.

The influence of the concentration was investigated by fabricating devices of different concentrations (1, 3, 5, 15, and 30 mM) of DB24C8 (Fig. S1) and monitoring their photovoltaic characteristics, namely, short-circuit current density (J_{SC}), open-circuit voltage (V_{OC}), fill factor (FF), and power conversion efficiency (PCE). The effect of the concentration on the performance differed depending on the perovskite composition (Table S1). The performance of MA-based devices was reduced upon treatment compared to the control (about 91%–96% PCE of the control on average), which was more pronounced at higher concentrations (average 37%–52% PCE of the control), thereby focusing on the lowest concentration (3 mM) in $MAPbI_3$ solar cells [Fig. S1(a)]. On the contrary, in MA-free PSCs, higher concentrations were beneficial for device performance. Specifically, higher concentrations (15 and 30 mM) significantly enhanced both V_{OC} and FF, leading to improved PCEs, identifying 15 mM as the optimal concentration for MA-free devices [Fig. S1(b) and Table S1]. This was in good agreement with the previous reports employing DB24C8 in FA-based PSCs.[24]

Further studies were performed to gain a deeper understanding of these effects. The assemblies of the crown ether moieties and their effect on the surface morphology were inspected via atomic force microscopy (AFM). In both perovskite compositions, the treatment initiated the formation of nanostructures on the surface of the perovskites (Fig. 2), which could be associated with assem-

23 May 2025 19:30:30

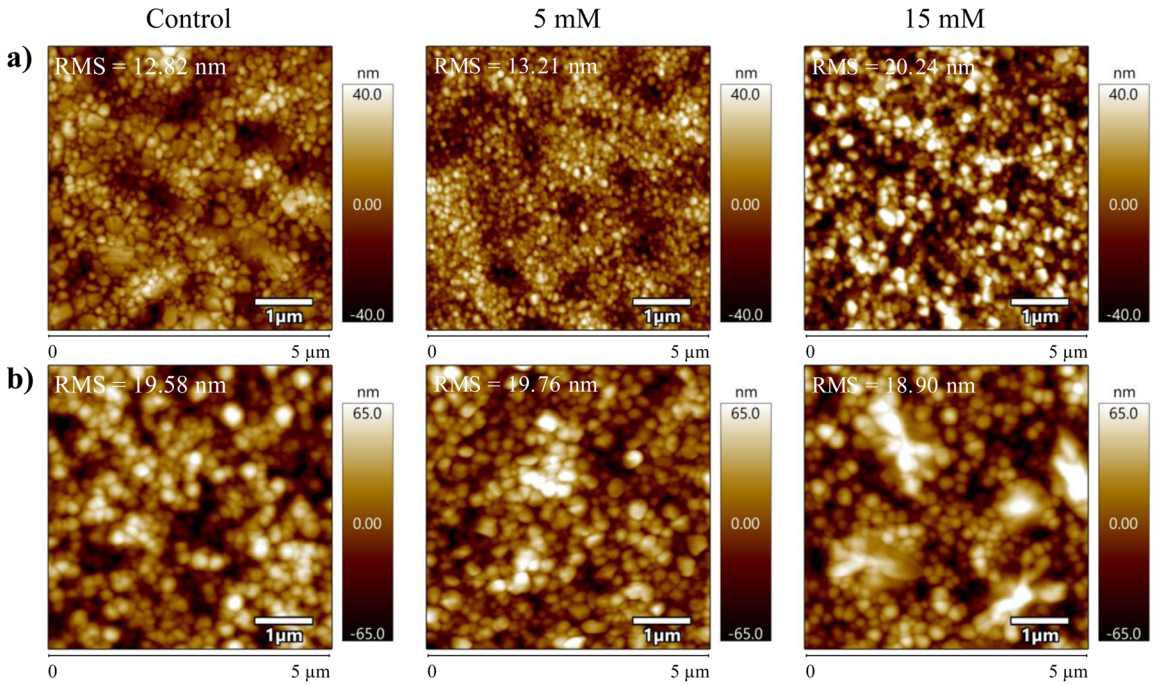

FIG. 2. AFM images showing the surface morphology of control and post-treated (a) $MAPbI_3$ and (b) $Cs_{0.1}FA_{0.9}PbI_{2.55}Br_{0.45}$ perovskite films on glass/ITO/NiO_x substrates. The samples were post-treated using 5 and 15 mM solutions of DB24C8 in CB. Root mean square (RMS) roughness values are shown as an inset.

© Author(s) 2024

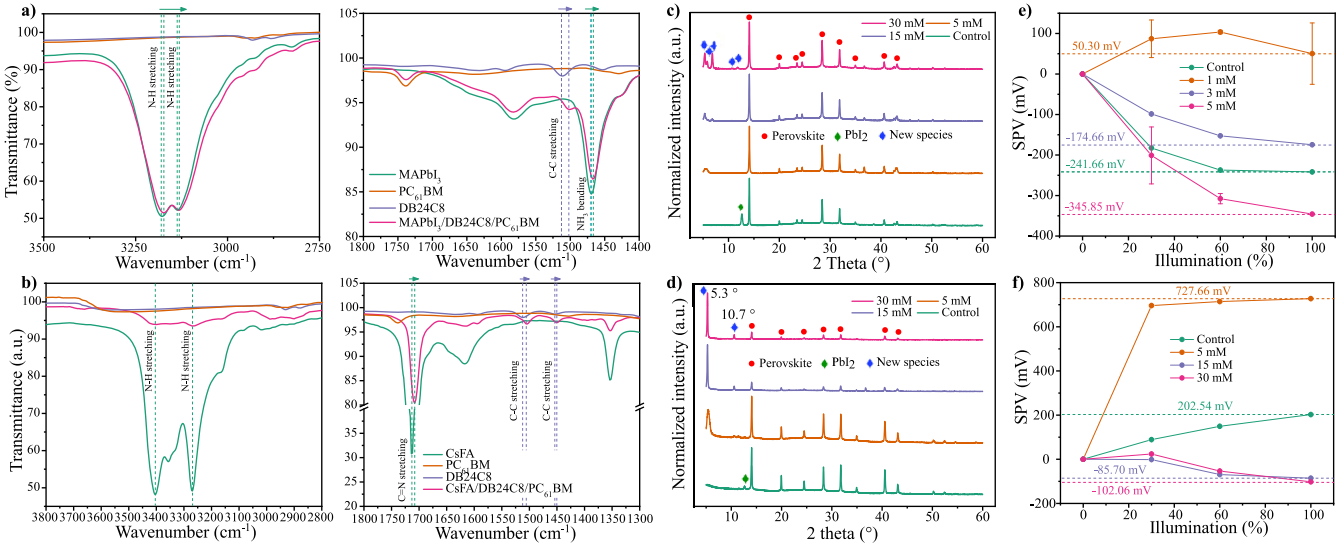

FIG. 3. ATR-FTIR results showing shifts in bands corresponding to perovskite and DB24C8 in (a) $MAPbI_3$/DB24C8/$PC_{61}BM$ and (b) $Cs_{0.1}FA_{0.9}PbI_{2.55}Br_{0.45}$/DB24C8/$PC_{61}BM$ systems. XRD patterns of control and post-treated (c) $MAPbI_3$ and (d) $Cs_{0.1}.FA_{0.9}PbI_{2.55}Br_{0.45}$ films on glass/ITO/NiO_x substrates. SPV as a function of illumination power (in % of the white LED source controled by AFM software) for control and post-treated (e) $MAPbI_3$ and (f) $Cs_{0.1}.FA_{0.9}PbI_{2.55}Br_{0.45}$ on ITO/NiO_x substrates.

blies of crown ethers that were previously reported.[24,25,39,42] The nanostructures on the surface of MA-based perovskite films formed clusters [Fig. 2(a)], whereas the ones on the MA-free perovskite films displayed a splatter-like appearance [Fig. 2(b)]. The size of these structures was dependent on the concentration of DB24C8, and they influenced the roughness of the perovskite films differently, i.e., the clusters in the MA-based films increased the roughness considerably (from 12.82 nm in the control to 20.24 when the film was post-treated using a 15 mM solution). In comparison, in the MA-free film, a slight decrease in surface roughness was observed in the presence of splatter-like structures (from 19.58 nm in the control to 18.9 when the film was post-treated using a 15 mM solution).[25,42] These changes in roughness were correlated with the observed changes in device performance as the higher roughness in the MA-based devices when using high DB24C8 concentrations (15 and 30 mM) likely contributed to poor interfacial contact with the electron-transporting layer ($PC_{61}BM$), influencing the performance.[43,44] In contrast, the improved film morphology in MA-free PSCs resulted in the opposite effect, benefiting the device performances.

To gain insight into the interaction between the crown ether assemblies and the perovskite layer, further investigation was performed by ATR-FTIR spectroscopy of thin films on glass substrates [Figs. 3(a) and 3(b)]. The samples consisting of perovskite materials (MA-based and MA-free), $PC_{61}BM$, and DB24C8, were studied and compared to identify the underlying interactions. The neat MA-based perovskite films displayed bands corresponding to N–H stretching at 3176 and 3135 cm^{-1}, along with $–NH_3$ bending at 1581 and 1469 cm^{-1} [Fig. S2(a)],[45] whereas the MA-free perovskite showed bands corresponding to N–H stretching (3404 and 3270 cm^{-1}), C=N stretching (1714 cm^{-1}), N–H bending (1620 cm^{-1}), and C–N stretching at 1354 cm^{-1} [Fig. S2(b)].[46] The $PC_{61}BM$ displayed distinct bands corresponding to C=O (1738 cm^{-1})[47] and CH_2 bending at 1429 cm^{-1}[48] [Fig. S2(c)], while DB24C8 showed three signatures corresponding to C–C stretching of the benzene ring (at 1595, 1512, and 1454 cm^{-1}) and one related to phenyl—O—C stretching at 1331 cm^{-1} [Fig. S2(d)].[49,50] In contrast, the stack of perovskite/DB24C8/$PC_{61}BM$, i.e., analogous to the one present in the solar cells, displayed shifts for some of the bands corresponding to the perovskite and the crown ether. Specifically, in the MA-based system, shifts toward lower wavenumbers in bands corresponding to the perovskite and the crown ether were observed corresponding to N–H stretching and $–NH_3$ bending from $MAPbI_3$ [indicated by green in Fig. 3(a)] and one band related to C–C stretching from DB24C8 [indicated by purple in Fig. 3(a)]. Similarly, in the MA-free system, comparable shifts were observed in the bands corresponding to C=N stretching from the perovskite [indicated by green in Fig. 3(b)] and those related to C–C stretching from DB24C8 [indicated by purple in Fig. 3(b)]. These results corroborate the interaction between DB24C8 host molecules and the perovskite film. However, no shifts were observed in the bands corresponding to $PC_{61}BM$, which points to the fact that the host–guest interaction is more selective, only affecting vibrational modes associated with the cations of the perovskite layer, with no significant interactions between DB24C8 and $PC_{61}BM$ when the crown ether was employed at the perovskite/$PC_{61}BM$ interface.

The structural characteristics of the crown ether assemblies were further assessed by means of x-ray diffraction (XRD) measurements. In the case of treated $MAPbI_3$ films, new peaks appeared

23 May 2025 19:30:30

© Author(s) 2024

at 11.8°, 10.7°, 6.8°, 5.8°, and 5.3° [Fig. 3(c)], while in the case of $Cs_{0.1}FA_{0.9}PbI_{2.55}Br_{0.45}$, only the new peaks at 5.3° and 10.7° appeared [Fig. 3(d)]. These low-angle peaks have also been reported previously in mixed-cation perovskite films treated with crown ethers.[24] It has also been reported that host–guest complexation between crown ethers and ammonium cations leads to the formation of different complexes displaying several XRD peaks at low angles.[51] This suggests that the nanostructures observed in our case might correspond to complexes formed via host–guest complexation between DB24C8 and the cations of the underlying perovskite layer. Furthermore, some degree of stacking might occur between DB24C8 molecules,[39] resulting in nanostructures with a higher out-of-plane height in the case of treated $MAPbI_3$ films. The distinct peaks observed in XRD patterns of both perovskite compositions of comparable concentration [Figs. 3(c) and 3(d)] point to different complexes, whereas the higher intensity observed in the MA-free perovskite [Fig. 3(d)] suggests a higher amount of crystalline structures affecting their morphology. These may arise from dissimilar crystallization routes and compositions, leading to different host–guest interactions. Furthermore, when treated with DB24C8, the intensity of the peak corresponding to PbI_2 in all perovskite films significantly decreased [Figs. 3(c) and 3(d)], suggesting an effect of DB24C8 on the stability of the materials.[52]

The nanostructures were assumed to influence the optoelectronic properties of the perovskite layers. Surface photovoltage (SPV) measurements were performed on thin films illuminated with different light intensities (dark, 30%, 60%, and 100% of the maximum power of the white LED source), demonstrating changes in the density of surface trap states upon post-treatment. The sign of the SPV corresponds to the nature of the trap states, i.e., whether they are acceptor-type (negative SPV, accumulate electrons) or donor-type (positive SPV, accumulate holes), and its magnitude qualitatively indicates the density of these trap states.[53,54] In the case of $MAPbI_3$, a low concentration of DB24C8 (1 mM) decreased the density of surface trap states but altered its type compared to the control, shifting them from acceptor-type to donor-type. Instead, increasing the concentration to 3 and 5 mM maintained the same type of trap states as the control (acceptor-type), whereas higher concentration led to an increase in their density [Fig. 3(c)]. On the contrary, when a low concentration of DB24C8 (5 mM) was employed in the MA-free perovskite, no change in the type of surface trap state was observed, but a significant increase in their density occurred. Conversely, increasing the concentration to 15 and 30 mM changed the type of trap states (from donor- to acceptor-) while simultaneously decreasing their density [Fig. 3(d)]. Accordingly, higher amounts of crown ether were beneficial when employing the MA-free perovskites but detrimental for MA-based perovskites.

Steady-state PL measurements further corroborated this. Perovskite films with and without $PC_{61}BM$ on top were to observe changes in charge extraction via quenching. Upon treatment with DB24C8, increased PL intensity was observed in both MA-based and MA-free compositions [Figs. 4(a) and 4(b)], indicating reduced non-radiative recombination. Interestingly, in MA-free perovskite, this increase in PL intensity reached a maximum when employing a concentration of 15 mM, being in accordance with the best-performing condition previously found [Fig. S1(b) and Table S2]. In the case of the MA-based perovskite, changes in the PL quenching showed hampered charge extraction from the perovskite to the electron transporting layer [Fig. 4(c)]. Increasing DB24C8 concentration led to an additional PL signal appearing [insets in Fig. 4(c)], which might be related to the observed nanostructures [Fig. 2(a)]. This might cause charge recombination in the nanostructures instead of their migration from the perovskite to the $PC_{61}BM$ layer, which results in reduced device performance with high post-treatment concentration, being in good agreement with the PV results [Fig. S1(a) and Table S1]. Overall, this suggests that a suitable amount of DB24C8 can contribute to defect passivation, leading to a decrease in the density of trap states at the perovskite/$PC_{61}BM$ interface.

The passivation effect was ascribed to the host–guest interactions of DB24C8 that could suppress some of the interfacial defects.[39] The main defects in the perovskite crystal structure, i.e., vacancies, interstitial, and antisite defects,[55] constitute different energy states capable of trapping charge carriers.[56] Their formation energy is highly dependent on the perovskite composition,[57,58] and deep-level states are the most problematic,[56] limiting the performance of devices. The nature of deep-level trap states is also dependent on composition, e.g., in $MAPbI_3$, the major source of these states are Pb_I antisites, which trap electrons,[58] whereas in $FAPbI_3$, FA_I and I_{FA} antisites are the main ones responsible for electron- and hole-trapping, respectively.[59] Crown ethers were shown to be capable of passivating FA^+ ionic defects, e.g., FA_i^+ and FA_I antisites[24] and also Pb_I antisites, among other defects.[60] Through this process, DB24C8-mediated surface modulation could successfully decrease the density of trap states in both MA-based and MA-free devices, corroborating the optoelectronic characteristics of the films. Although theoretical calculations in the literature reports suggested that crown ethers can passivate both donor- and acceptor-type trap states,[60] experimental evidence indicates that they are more likely to passivate acceptor-type defects.[24,60] This explains the shift in trap state type observed in SPV measurements (Fig. 3). While the surface of the perovskite film of the devices contained both donor- and acceptor-type trap states, upon treatment with the optimal concentration of DB24C8, most of the acceptor-type ones were passivated, i.e., the remaining ones are donor-type, in accordance with the positive signal observed in the SPV plots for low concentration post-treatment regardless of the perovskite composition [Figs. 3(e) and 3(f)]. Further increasing the concentration leads to the formation of surface nanostructures (Fig. 2), which could behave as acceptor-type traps, increasing the density of trap states with concentration [Figs. 3(e) and 3(f)]. This leads to an optimal concentration for each perovskite composition (Fig. 5). However, the origin of the significant increase in the density of trap states upon low concentration post-treatment of the MA-free perovskite remains elusive. On the other hand, the reason behind the difference in the optimum concentration for effective passivation between the two perovskites might be related to how favorable the host–guest interactions between DB24C8 and the defect are, which depends on the nature of the interaction.[61,62] Therefore, effective passivation of deep-level traps in the MA-based perovskite appears to be the most favorable interaction, leading to a low amount of crown ether required when compared to the MA-free perovskite.

23 May 2025 19:30:30

© Author(s) 2024

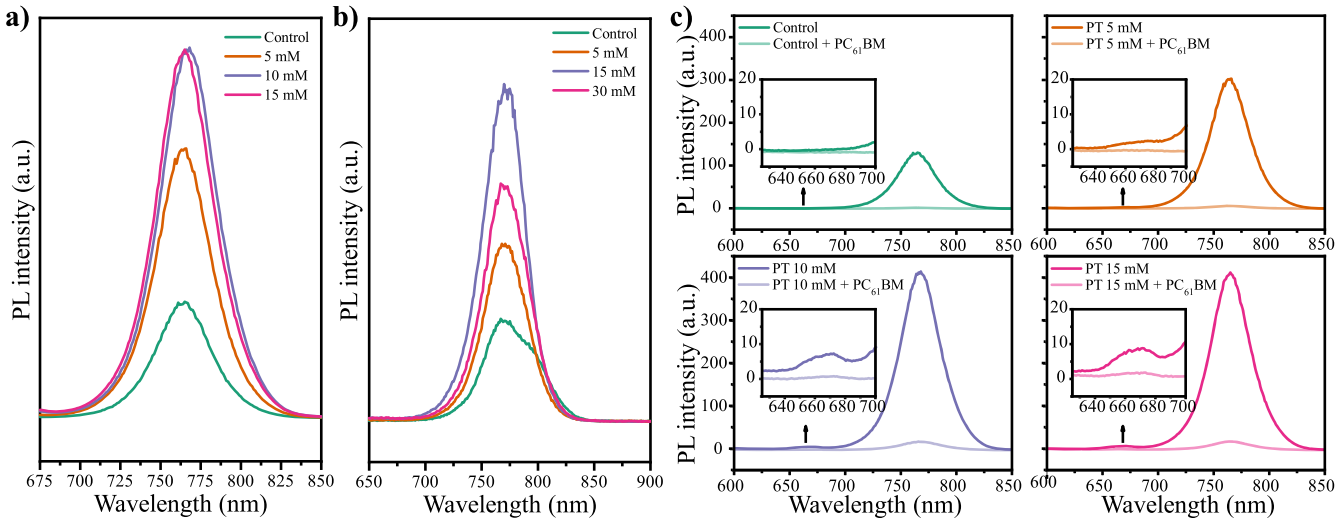

FIG. 4. Steady-state PL measurements of control and post-treated (a) $MAPbI_3$ and (b) $Cs_{0.1}FA_{0.9}PbI_{2.55}Br_{0.45}$ films on glass/ITO/NiOx substrates. (c) Steady-state PL measurements of control and post-treated $MAPbI_3$ films on glass/ITO/NiO_x substrates, both with and without $PC_{61}BM$ on top of the perovskite layer, showing a quenching effect. The insets show the PL signal likely attributed to nanostructures in $MAPbI_3$ perovskite.

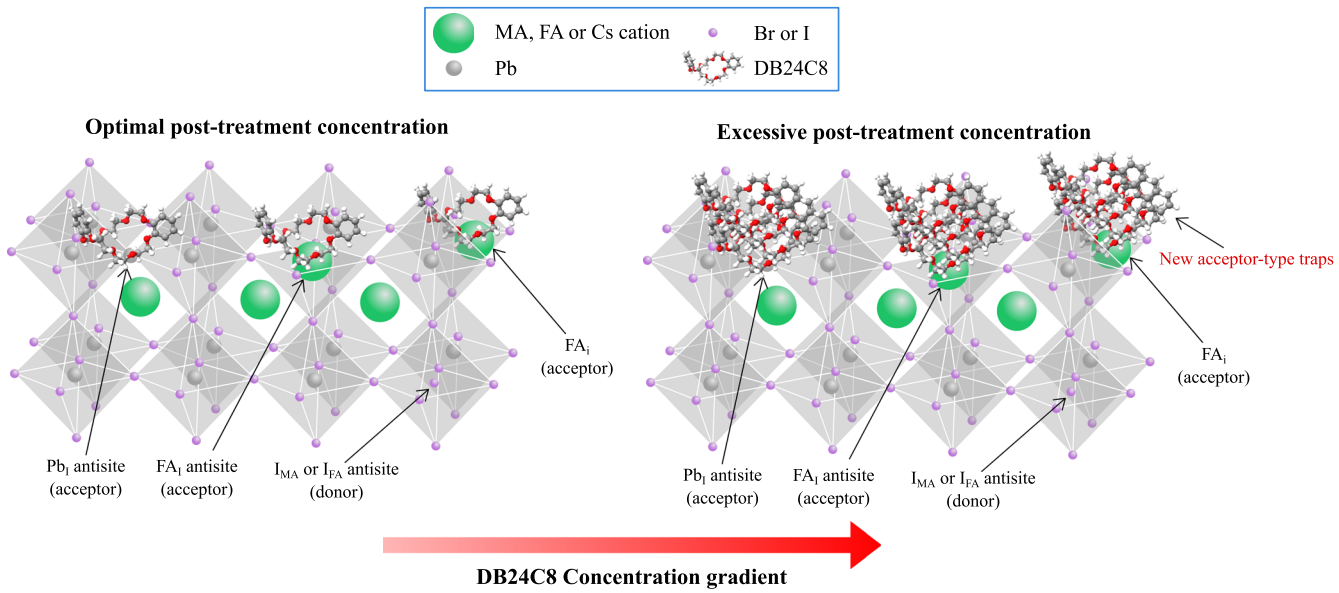

FIG. 5. Schematic representation of surface modulation via DB24C8-mediated host–guest complexation on the perovskite surface showing differences between the conditions.

Finally, we hypothesized that DB24C8 could also display interactions with $PC_{61}BM$ in the precursor solution and at the interface. For this reason, DB24C8 was analyzed as an additive to the $PC_{61}BM$ layer in the bulk of the precursor solution in a low concentration (1 mM) and employed for the fabrication of inverted solar cells using both perovskite compositions. In the case of $MAPbI_3$, an improvement was observed compared to the control due to increased FF (Table S3), while exactly the opposite was observed in devices fabricated using the MA-free perovskite (Table S4). The ^{1}H-NMR measurements performed using deuterated toluene (toluene-d_8) and deuterated chloroform ($CDCl_3$) showed that no significant chemical interaction took place between the crown ether and the $PC_{61}BM$ in solution (Fig. S3), indicating that no apparent host–guest interactions were taking place in the precursor solution. Thereby we

23 May 2025 19:30:30

© Author(s) 2024

attribute the observed changes in photovoltaic parameters to the changes in the interfacial assemblies that are beyond the scope of this work, which is expected to affect operational stabilities.

B. Stability enhancement by host–guest complexation

The stability of inverted PSCs with DB24C8 post-treatment was tested following both ISOS-D-2I and ISOS-L-2I protocols, i.e., subjecting the devices to constant heating at 65 °C inside a N_2-filled glovebox and to constant heating at the same temperature and continuous illumination under 1 sun employing a solar simulator.[34]

The ISOS-D-2I test was performed for over 500 h, and devices were fabricated using the optimal crown ether concentration (3 and 15 mM for MA-based and MA-free PSCs, respectively) and compared to untreated control samples. In the case of MA-based devices, the treated condition (3 mM) yielded more stable solar cells, which, on average, were able to retain 77% of their initial PCE after the test, while the control only retained 51% of its initial PCE [Fig. 6(a) and Table S5]. A similar trend was observed in MA-free PSCs, where the treated condition (15 mM) retained 97% of its initial PCE after the test, while the control retained 85% of its initial PCE [Fig. 6(b) and Table S5]. During this test, the structural changes were assessed by monitoring the intensity ratios between the peaks corresponding to PbI_2 and perovskite phases, which were calculated from the XRD measurements (Fig. S4). Unlike the control samples, none of the treated samples showed the formation of PbI_2 over time, which suggests that no significant degradation of the perovskite material occurred. This was also the case for the MA-free control devices, which is in good agreement with their higher thermal stability (Fig. S4). Instead, in the control MA-based samples, PbI_2 was formed over time, suggesting more pronounced degradation in these materials under operating conditions. The overall better results obtained with the MA-free devices are due to the better thermal stability of FA-based perovskites.[9,10] Furthermore, the treated conditions displayed a narrower value distribution, indicating an improvement in the reproducibility of the results upon the use of host–guest complexation. These results suggest that the drop in PCE observed in the samples during the stability test was not directly caused by changes in the properties of the perovskite material due to decomposition, as indicated by the XRD measurements (Fig. S4). Instead, the degradation was more likely to be related to the subsequent layers of the devices (i.e., $PC_{61}BM$ and silver electrode), which could be responsible for the decreased performance of the devices over time, such as through the corrosion of silver electrode due to the migration of iodide through the $PC_{61}BM$ to the electrode and simultaneous reduction of the electron extraction capability at the perovskite/$PC_{61}BM$ interface.[63,64] After the ISOS-D-2I stability test, the PSCs displayed degraded silver electrodes (Fig. S5), which indicates that the PCE of the devices decreased mainly due to the contact layers. The approach was more effective upon independently stabilizing the contacts through the assembly of the crown ether moieties since the stability of devices fabricated by doping the $PC_{61}BM$ layer with DB24C8 (1 mM concentration) was not effective (Fig. S6). Therefore, the improvement in the stability of the post-treated device is likely to be caused by the ion binding capabilities of DB24C8, enabling the assembled molecule

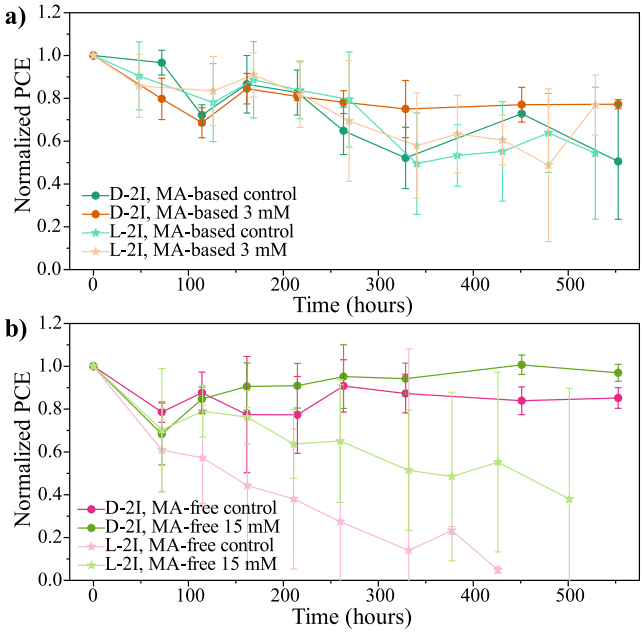

FIG. 6. Normalized PCE over time of (a) MA-based and (b) MA-free PSCs subjected to ISOS-D-2I (65 °C in N_2 atmosphere) and ISOS-L-2I (65 °C in N_2 the atmosphere under simulated sunlight) stability tests.

to act as a blocking layer for the migration of compounds and ions from the perovskite[65] through the $PC_{61}BM$ to the silver electrode, thus retarding the degradation of the contact layers and increasing operational stability. These results compare well to others in the literature, mostly focused on n-i-p architectures (Table S6). On the other hand, when subjected to ISOS-L-2I tests at elevated temperatures, no significant difference could be observed after 500 h between the control and treated MA-based devices since they retained, on average, 54% and 77% of their initial PCE, respectively [Fig. 6(a)]. However, in the case of MA-free devices, more noticeable differences appeared since the control was only able to operate for over 400 h (retaining 5% of the initial PCE on average), after which the devices stopped working. In contrast, the treated devices operated for over 400 h, retaining about 40% of the initial PCE on average [Fig. 6(b)]. This showcases the superior stabilities for MA-free perovskites upon crown ether modulation in p-i-n architectures at elevated temperatures (Table S6), highlighting the potential of the approach.

IV. CONCLUSIONS

In summary, interfacial modulation via host–guest complexation was identified as a versatile strategy to improve the stability of inverted PSCs employing materials with different compositions as light absorbers, including $MAPbI_3$ and $Cs_{0.1}FA_{0.9}PbI_{2.55}Br_{0.45}$. For this purpose, DB24C8 was used in the treatment of the perovskite films in solar cell devices. Upon treatment, molecules of DB24C8 displayed host–guest interactions with the underlying perovskite

23 May 2025 19:30:30

© Author(s) 2024

layer, forming complexes whose nature was influenced by the composition of the perovskite, ultimately leading to the formation of nanostructures with different morphologies that were dependent on the concentration of the solution for the treatment. In the case of MA-based inverted PSCs, high concentrations (>5 mM) of DB24C8 led to a decrease in PCE since charge extraction from the perovskite material to the electron transporting layer was hindered, and the density of trap states at the perovskite/$PC_{61}BM$ interface increased, as revealed by the PL and SPV measurements. Instead, using lower concentrations (<5 mM) of the crown ether limited the formation of these nanostructures, thus maintaining the performance of the devices. Conversely, in the MA-free PSCs, a higher concentration of DB24C8 in the post-treatment (15 and 30 mM) led to increased PCE, whereas a lower concentration (<15 mM) hampered the device performance, which was related to the passivation of deep-level trap states via host–guest interactions, leading to reduced density of surface trap states at the perovskite/$PC_{61}BM$ interface.

As a result, ISOS-D-I2 stability tests of inverted PSCs demonstrated that using DB24C8 post-treatment of the perovskite film in the devices successfully increased their stability regardless of the employed perovskite material. The treated MA-based and MA-free PSCs were able to retain 77% and 97% of their initial PCE on average after more than 500 h, respectively, which was superior when compared to 51% and 85% for the corresponding control devices. Additional ISOS-L-2I tests also demonstrated the enhanced stability of treated devices, especially in the MA-free devices. We provide complementary mechanistic insights on the molecular-level interactions enabling the photovoltaic performances and operational stabilities. Specifically, the improvement was related to the ion binding capabilities of DB24C8, which enable the molecule to act as a blocking layer for the migration of ions from the perovskite through the $PC_{61}BM$ to the silver electrode, thus retarding the degradation of the contact layers in the resulting solar cells. This provides a versatile strategy for advancing the performances and long-term stability of these solar cell devices toward practical applications, which requires scaling up the approach and adapting it to the existing manufacturing processes that is the subject of our ongoing investigations. While the resulting photovoltaic performances can be further optimized, our findings provide new insights into the use of supramolecular strategies in advancing perovskite solar cell research for the next-generation perovskite solar cells.

SUPPLEMENTARY MATERIAL

Complementary characterization is available in the supplementary material (Figs. S1–S6 and Tables S1–S6).

ACKNOWLEDGMENTS

We acknowledge the Swiss Leading House for the Latin American Region and Research Partnership Grant No. 2126.

AUTHOR DECLARATIONS

Conflict of Interest

The authors have no conflicts to disclose.

Author Contributions

Kevin Ballestas: Data curation (lead); Investigation (lead); Methodology (equal); Validation (equal); Visualization (equal); Writing – original draft (lead); Writing – review & editing (equal). **Jovana V. Milić**: Conceptualization (lead); Funding acquisition (equal); Resources (equal); Supervision (equal); Writing – review & editing (equal). **Daniel Ramírez**: Conceptualization (equal); Funding acquisition (equal); Investigation (equal); Resources (equal); Supervision (equal); Writing – review & editing (equal).

DATA AVAILABILITY

Data can be accessed at the DOI:10.5281/zenodo.11222473 and it is available under the license CC-BY-4.0 (Creative Commons Attribution-ShareAlike 4.0 International).

REFERENCES

[1] NREL, Best Research-Cell Efficiency Chart, 2024.
[2] Q. Dong, Y. Fang, Y. Shao, P. Mulligan, J. Qiu, L. Cao, and J. Huang, "Electron-hole diffusion lengths > 175 μm in solution-grown $CH_3NH_3PbI_3$ single crystals," Science **347**, 967–970 (2015).
[3] S. D. Stranks, G. E. Eperon, G. Grancini, C. Menelaou, M. J. P. Alcocer, T. Leijtens, L. M. Herz, A. Petrozza, and H. J. Snaith, "Electron-hole diffusion lengths exceeding 1 micrometer in an organometal trihalide perovskite absorber," Science **342**, 341–344 (2013).
[4] D. Shi, V. Adinolfi, R. Comin, M. Yuan, E. Alarousu, A. Buin, Y. Chen, S. Hoogland, A. Rothenberger, K. Katsiev, Y. Losovyj, X. Zhang, P. A. Dowben, O. F. Mohammed, E. H. Sargent, and O. M. Bakr, "Low trap-state density and long carrier diffusion in organolead trihalide perovskite single crystals," Science **347**, 519–522 (2015).
[5] H. S. Jung, G. S. Han, N.-G. Park, and M. J. Ko, "Flexible perovskite solar cells," Joule **3**, 1850–1880 (2019).
[6] K. Xu, A. Al-Ashouri, Z.-W. Peng, E. Köhnen, H. Hempel, F. Akhundova, J. A. Marquez, P. Tockhorn, O. Shargaieva, F. Ruske, J. Zhang, J. Dagar, B. Stannowski, T. Unold, D. Abou-Ras, E. Unger, L. Korte, and S. Albrecht, "Slot-die coated triple-halide perovskites for efficient and scalable perovskite/silicon tandem solar cells," ACS Energy Lett. **7**, 3600–3611 (2022).
[7] K. Lin, J. Xing, L. N. Quan, F. P. G. de Arquer, X. Gong, J. Lu, L. Xie, W. Zhao, D. Zhang, C. Yan, W. Li, X. Liu, Y. Lu, J. Kirman, E. H. Sargent, Q. Xiong, and Z. Wei, "Perovskite light-emitting diodes with external quantum efficiency exceeding 20 per cent," Nature **562**, 245–248 (2018).
[8] M. Grätzel, "The light and shade of perovskite solar cells," Nat. Mater. **13**, 838–842 (2014).
[9] G. E. Eperon, S. D. Stranks, C. Menelaou, M. B. Johnston, L. M. Herz, and H. J. Snaith, "Formamidinium lead trihalide: A broadly tunable perovskite for efficient planar heterojunction solar cells," Energy Environ. Sci. **7**, 982–988 (2014).
[10] Z. Liu, P. Liu, M. Li, T. He, T. Liu, L. Yu, and M. Yuan, "Efficient and stable FA-rich perovskite photovoltaics: From material properties to device optimization," Adv. Energy Mater. **12**, 2200111 (2022).
[11] J. Park, J. Kim, H.-S. Yun, M. J. Paik, E. Noh, H. J. Mun, M. G. Kim, T. J. Shin, and S. I. Seok, "Controlled growth of perovskite layers with volatile alkylammonium chlorides," Nature **616**, 724–730 (2023).
[12] W. Fu, A. G. Ricciardulli, Q. A. Akkerman, R. A. John, M. M. Tavakoli, S. Essig, M. V. Kovalenko, and M. Saliba, "Stability of perovskite materials and devices," Mater. Today **58**, 275–296 (2022).
[13] J. Zhuang, J. Wang, and F. Yan, "Review on chemical stability of lead halide perovskite solar cells," Nano-Micro Lett. **15**, 84 (2023).
[14] X. Lin, D. Cui, X. Luo, C. Zhang, Q. Han, Y. Wang, and L. Han, "Efficiency progress of inverted perovskite solar cells," Energy Environ. Sci. **13**, 3823–3847 (2020).

23 May 2025 19:30:30

© Author(s) 2024

[15]R. Azmi, D. S. Utomo, B. Vishal, S. Zhumagali, P. Dally, A. M. Risqi, A. Prasetio, E. Ugur, F. Cao, I. F. Imran, A. A. Said, A. R. Pininti, A. S. Subbiah, E. Aydin, C. Xiao, S. I. Seok, and S. De Wolf, "Double-side 2D/3D heterojunctions for inverted perovskite solar cells," Nature **628**, 93–98 (2024).
[16]F. Zhang and K. Zhu, "Additive engineering for efficient and stable perovskite solar cells," Adv. Energy Mater. **10**, 1902579 (2020).
[17]X. Liu, D. Luo, Z.-H. Lu, J. S. Yun, M. Saliba, S. I. Seok, and W. Zhang, "Stabilization of photoactive phases for perovskite photovoltaics," Nat. Rev. Chem. **7**, 462–479 (2023).
[18]A. R. b. Mohd Yusoff, M. Vasilopoulou, D. G. Georgiadou, L. C. Palilis, A. Abate, and M. K. Nazeeruddin, "Passivation and process engineering approaches of halide perovskite films for high efficiency and stability perovskite solar cells," Energy Environ. Sci. **14**, 2906–2953 (2021).
[19]J. W. Steed, "First- and second-sphere coordination chemistry of alkali metal crown ether complexes," Coord. Chem. Rev. **215**, 171–221 (2001).
[20]D. Landini, A. Maia, F. Montanari, and F. M. Pirisi, "Crown ethers as phase-transfer catalysts. A comparison of anionic activation in aqueous–organic two-phase systems and in low polarity anhydrous solutions by perhydrodibenzo-18-crown-6, lipophilic quaternary salts, and cryptands," J. Chem. Soc., Perkin Trans. 2 **1980**, 46–51.
[21]K. Kimura, S. Kitazawa, T. Maeda, and T. Shono, "Cation-binding properties of poly- and bis(benzo-21-crown-7)derivatives," Fresenius' Z. Anal. Chem. **313**, 132–136 (1982).
[22]S. Bhattacharya, A. Sharma, S. K. Nayak, S. Chattopadhyay, and A. K. Mukherjee, "NMR study of complexation of crown ethers with [60]- and [70]fullerenes," J. Phys. Chem. B **107**, 4213–4217 (2003).
[23]P. Ferdowsi, U. Steiner, and J. V. Milić, "Host-guest complexation in hybrid perovskite optoelectronics," J. Phys. Mater. **4**, 042011 (2021).
[24]T.-S. Su, F. T. Eickemeyer, M. A. Hope, F. Jahanbakhshi, M. Mladenović, J. Li, Z. Zhou, A. Mishra, J.-H. Yum, D. Ren, A. Krishna, O. Ouellette, T.-C. Wei, H. Zhou, H.-H. Huang, M. D. Mensi, K. Sivula, S. M. Zakeeruddin, J. V. Milić, A. Hagfeldt, U. Rothlisberger, L. Emsley, H. Zhang, and M. Grätzel, "Crown ether modulation enables over 23% efficient formamidinium-based perovskite solar cells," J. Am. Chem. Soc. **142**, 19980–19991 (2020).
[25]R. Chen, Y. Wu, Y. Wang, R. Xu, R. He, Y. Fan, X. Huang, J. Yin, B. Wu, J. Li, and N. Zheng, "Crown ether-assisted growth and scaling up of $FACsPbI_3$ films for efficient and stable perovskite solar modules," Adv. Funct. Mater. **31**, 2008760 (2021).
[26]K. Chen, H. Lu, Y. Yang, S. Li, K. Jia, F. Wu, and L. Zhu, "Simultaneously modifying hole transport material and perovskite via a crown ether-based semiconductor toward efficient and stable perovskite solar cells," Sol. RRL **7**, 2200987 (2023).
[27]Y. Huang, A. Aierken, G. Yu, W. Zhang, S. Wang, Y. Sui, J. Tang, X. Yang, Y. Zhuang, Q. Song, and Z. Tang, "Enhanced efficiency and stability of perovskite solar cells achieved by incorporating potassium cation-18-crown ether-6 complexes," Org. Electron. **116**, 106766 (2023).
[28]M.-G. La-Placa, L. Gil-Escrig, D. Guo, F. Palazon, T. J. Savenije, M. Sessolo, and H. J. Bolink, "Vacuum-deposited 2D/3D perovskite heterojunctions," ACS Energy Lett. **4**, 2893–2901 (2019).
[29]D. Koushik, W. J. H. Verhees, Y. Kuang, S. Veenstra, D. Zhang, M. A. Verheijen, M. Creatore, and R. E. I. Schropp, "High-efficiency humidity-stable planar perovskite solar cells based on atomic layer architecture," Energy Environ. Sci. **10**, 91–100 (2017).
[30]H. C. Weerasinghe, N. Macadam, J.-E. Kim, L. J. Sutherland, D. Angmo, L. W. T. Ng, A. D. Scully, F. Glenn, R. Chantler, N. L. Chang, M. Dehghanimadvar, L. Shi, A. W. Y. Ho-Baillie, R. Egan, A. S. R. Chesman, M. Gao, J. J. Jasieniak, T. Hasan, and D. Vak, "The first demonstration of entirely roll-to-roll fabricated perovskite solar cell modules under ambient room conditions," Nat. Commun. **15**, 1656 (2024).
[31]J. Li, J. Dagar, O. Shargaieva, M. A. Flatken, H. Köbler, M. Fenske, C. Schultz, B. Stegemann, J. Just, D. M. Többens, A. Abate, R. Munir, and E. Unger, "20.8% slot-die coated $MAPbI_3$ perovskite solar cells by optimal DMSO-content and age of 2-ME based precursor inks," Adv. Energy Mater. **11**, 2003460 (2021).
[32]T. Du, S. Qiu, X. Zhou, V. M. Le Corre, M. Wu, L. Dong, Z. Peng, Y. Zhao, D. Jang, E. Spiecker, C. J. Brabec, and H.-J. Egelhaaf, "Efficient, stable, and fully printed carbon-electrode perovskite solar cells enabled by hole-transporting bilayers," Joule **7**, 1920–1937 (2023).
[33]S. J. Kim, R. Kumar Chitumalla, J. M. Kim, J. Jang, J. W. Oh, J. V. Milić, and J. Y. Seo, "Controlled growth of hybrid halide perovskites by crown ether complexation for perovskite solar cells," Helv. Chim. Acta **106**, e202200193 (2023).
[34]M. V. Khenkin, E. A. Katz, A. Abate, G. Bardizza, J. J. Berry, C. Brabec, F. Brunetti, V. Bulović, Q. Burlingame, A. Di Carlo, R. Cheacharoen, Y.-B. Cheng, A. Colsmann, S. Cros, K. Domanski, M. Dusza, C. J. Fell, S. R. Forrest, Y. Galagan, D. Di Girolamo, M. Grätzel, A. Hagfeldt, E. von Hauff, H. Hoppe, J. Kettle, H. Köbler, M. S. Leite, S. (Frank) Liu, Y.-L. Loo, J. M. Luther, C.-Q. Ma, M. Madsen, M. Manceau, M. Matheron, M. McGehee, R. Meitzner, M. K. Nazeeruddin, A. F. Nogueira, Ç. Odabaşı, A. Osherov, N.-G. Park, M. O. Reese, F. De Rossi, M. Saliba, U. S. Schubert, H. J. Snaith, S. D. Stranks, W. Tress, P. A. Troshin, V. Turkovic, S. Veenstra, I. Visoly-Fisher, A. Walsh, T. Watson, H. Xie, R. Yıldırım, S. M. Zakeeruddin, K. Zhu, and M. Lira-Cantu, "Consensus statement for stability assessment and reporting for perovskite photovoltaics based on ISOS procedures," Nat. Energy **5**, 35–49 (2020).
[35]J. Ciro, D. Ramírez, M. A. Mejía Escobar, J. F. Montoya, S. Mesa, R. Betancur, and F. Jaramillo, "Self-functionalization behind a solution-processed NiO_x film used as hole transporting layer for efficient perovskite solar cells," ACS Appl. Mater. Interfaces **9**, 12348–12354 (2017).
[36]M. Saliba, J. P. Correa-Baena, C. M. Wolff, M. Stolterfoht, N. Phung, S. Albrecht, D. Neher, and A. Abate, "How to make over 20% efficient perovskite solar cells in regular (n-i-p) and inverted (p-i-n) architectures," Chem. Mater. **30**, 4193–4201 (2018).
[37]V. Panchal, R. Pearce, R. Yakimova, A. Tzalenchuk, and O. Kazakova, "Standardization of surface potential measurements of graphene domains," Sci. Rep. **3**, 2597 (2013).
[38]J. Ciro, S. Mesa, J. I. Uribe, M. A. Mejía-Escobar, D. Ramirez, J. F. Montoya, R. Betancur, H.-S. Yoo, N.-G. Park, and F. Jaramillo, "Optimization of the Ag/PCBM interface by a rhodamine interlayer to enhance the efficiency and stability of perovskite solar cells," Nanoscale **9**, 9440–9446 (2017).
[39]H. Zhang, F. T. Eickemeyer, Z. Zhou, M. Mladenović, F. Jahanbakhshi, L. Merten, A. Hinderhofer, M. A. Hope, O. Ouellette, A. Mishra, P. Ahlawat, D. Ren, T. S. Su, A. Krishna, Z. Wang, Z. Dong, J. Guo, S. M. Zakeeruddin, F. Schreiber, A. Hagfeldt, L. Emsley, U. Rothlisberger, J. V. Milić, and M. Grätzel, "Multimodal host–guest complexation for efficient and stable perovskite photovoltaics," Nat. Commun. **12**, 3383 (2021).
[40]S. Bhattacharya, A. Sharma, S. K. Nayak, and A. K. Mukherjee, "Vertical ionisation potentials of a number of crown ethers from charge transfer bands of their EDA complexes," Spectrochim. Acta, Part A **58**, 2841–2848 (2002).
[41]K. Datta, M. Banerjee, and A. K. Mukherjee, "Comparative study of the host–guest complexes of [60]- and [70]-fullerenes with *N,N*'-dibenzyl-1,4,10,13-tetraoxa-7,16-diaza-cyclooctadecane in different solvents," J. Phys. Chem. B **108**, 16100–16106 (2004).
[42]Y. Yang, T. Zhao, M.-H. Li, X. Wu, M. Han, S.-C. Yang, Q. Xu, L. Xian, X. Chi, N.-J. Zhao, H. Cui, S. Li, J.-S. Hu, B. Zhang, and Y. Jiang, "Passivation of positively charged cationic defects in perovskite with nitrogen-donor crown ether enabling efficient perovskite solar cells," Chem. Eng. J. **451**, 138962 (2023).
[43]M.-H. Li, F.-Z. Qiu, S. Wang, Y. Jiang, and J.-S. Hu, "Hole transporting materials in inorganic $CsPbI_{3-x}Br_x$ solar cells: Fundamentals, criteria and opportunities," Mater. Today **52**, 250–268 (2022).
[44]J. Tian, Q. Xue, X. Tang, Y. Chen, N. Li, Z. Hu, T. Shi, X. Wang, F. Huang, C. J. Brabec, H.-L. Yip, and Y. Cao, "Dual interfacial design for efficient $CsPbI_2Br$ perovskite solar cells with improved photostability," Adv. Mater. **31**, 1901152 (2019).
[45]M. A. Pérez-Osorio, R. L. Milot, M. R. Filip, J. B. Patel, L. M. Herz, M. B. Johnston, and F. Giustino, "Vibrational properties of the organic–inorganic halide perovskite $CH_3NH_3PbI_3$ from theory and experiment: Factor group analysis, first-principles calculations, and low-temperature infrared spectra," J. Phys. Chem. C **119**, 25703–25718 (2015).
[46]A. E. A. Bracesco, J. W. P. Jansen, H. Xue, V. Zardetto, G. Brocks, W. M. M. Kessels, S. Tao, and M. Creatore, "In situ IR spectroscopy studies of atomic layer-deposited SnO_2 on formamidinium-based lead halide perovskite," ACS Appl. Mater. Interfaces **15**, 38018–38028 (2023).

23 May 2025 19:30:30

© Author(s) 2024

[47]S. H. Yoo, J. M. Kum, and S. O. Cho, "Tuning the electronic band structure of PCBM by electron irradiation," Nanoscale Res. Lett. **6**, 545 (2011).
[48]G. Kalonga, K. Chinyama, O. Munyati, and M. Maaza, "Characterization and optimization of poly (3-hexylthiophene-2, 5- diyl) (P3HT) and [6, 6] phenyl-C61-butyric acid methyl ester (PCBM) blends for optical absorption," J. Chem. Eng. Mater. Sci. **4**, 93–102 (2013).
[49]M. Roy and M. Kundu, "Supramolecular assembly of ionic liquid with cyclic polyethers to form inclusion complexes," Indian J. Adv. Chem. Sci. **5**, 92–101 (2017).
[50]E. V. Guseva, T. E. Busygina, L. S. Gracheva, V. K. Polovnyak, R. A. Khasanshin, E. G. Yarkova, and R. A. Yusupov, "Complex formation of potassium hexachloroplatinate with 18-crown-6 and dibenzo-18-crown-6 in acetonitrile," Russ. J. Gen. Chem. **71**, 217–221 (2001).
[51]T. Chatterjee, M. Sarma, and S. K. Das, "Supramolecular architectures from ammonium-crown ether inclusion complexes in polyoxometalate association: Synthesis, structure, and spectroscopy," Cryst. Growth Des. **10**, 3149–3163 (2010).
[52]C.-J. Tong, W. Geng, Z.-K. Tang, C.-Y. Yam, X.-L. Fan, J. Liu, W.-M. Lau, and L.-M. Liu, "Uncovering the veil of the degradation in perovskite $CH_3NH_3PbI_3$ upon humidity exposure: A first-principles study," J. Phys. Chem. Lett. **6**, 3289–3295 (2015).
[53]L. Kronik and Y. Shapira, "Surface photovoltage spectroscopy of semiconductor structures: At the crossroads of physics, chemistry and electrical engineering," Surf. Interface Anal. **31**, 954–965 (2001).
[54]W. Zhang, S. Pathak, N. Sakai, T. Stergiopoulos, P. K. Nayak, N. K. Noel, A. A. Haghighirad, V. M. Burlakov, D. W. DeQuilettes, A. Sadhanala, W. Li, L. Wang, D. S. Ginger, R. H. Friend, and H. J. Snaith, "Enhanced optoelectronic quality of perovskite thin films with hypophosphorous acid for planar heterojunction solar cells," Nat. Commun. **6**, 10030 (2015).
[55]J. Xue, R. Wang, and Y. Yang, "The surface of halide perovskites from nano to bulk," Nat. Rev. Mater. **5**, 809–827 (2020).
[56]J. M. Ball and A. Petrozza, "Defects in perovskite-halides and their effects in solar cells," Nat. Energy **1**, 16149 (2016).
[57]N. Liu and C. Yam, "First-principles study of intrinsic defects in formamidinium lead triiodide perovskite solar cell absorbers," Phys. Chem. Chem. Phys. **20**, 6800–6804 (2018).
[58]A. Buin, R. Comin, J. Xu, A. H. Ip, and E. H. Sargent, "Halide-dependent electronic structure of organolead perovskite materials," Chem. Mater. **27**, 4405–4412 (2015).
[59]X. Yang, Y. Ni, Y. Zhang, Y. Wang, W. Yang, D. Luo, Y. Tu, Q. Gong, H. Yu, and R. Zhu, "Multiple-defect management for efficient perovskite photovoltaics," ACS Energy Lett. **6**, 2404–2412 (2021).
[60]P. Gao, Y. Ji, J. Song, G. Zhou, J. Lai, X. Yin, Y. Li, T. Song, Z. Zhao, Q. Chen, W. Feng, L. Chen, Y. Zhang, S. Yang, B. Sun, and F. Liu, "Crown ether-induced supramolecular passivation and two-dimensional crystal interlayer formation in perovskite photovoltaics," Cell Rep. Phys. Sci. **2**, 100450 (2021).
[61]L. Brunsveld, B. J. B. Folmer, E. W. Meijer, and R. P. Sijbesma, "Supramolecular polymers," Chem. Rev. **101**, 4071–4098 (2001).
[62]L. K. S. von Krbek, A. J. Achazi, S. Schoder, M. Gaedke, T. Biberger, B. Paulus, and C. A. Schalley, "The delicate balance of preorganisation and adaptability in multiply bonded host–guest complexes," Chem. Eur. J. **23**, 2877–2883 (2017).
[63]J. Li, Q. Dong, N. Li, and L. Wang, "Direct evidence of ion diffusion for the silver-electrode-induced thermal degradation of inverted perovskite solar cells," Adv. Energy Mater. **7**, 1602922 (2017).
[64]Y. Kato, L. K. Ono, M. V. Lee, S. Wang, S. R. Raga, and Y. Qi, "Silver iodide formation in methyl ammonium lead iodide perovskite solar cells with silver top electrodes," Adv. Mater. Interfaces **2**, 1500195 (2015).
[65]P. Ferdowsi, G. Bravetti, M. C. Schmidt, E. Ochoa-Martinez, S. Bijani, A. Rizzo, S. Colella, U. Steiner, B. Ehrler, D. J. Kubicki, and J. V. Milić, "Host–guest complexation in wide bandgap perovskite solar cells," Sol. RRL **8**, 2300655 (2024).

23 May 2025 19:30:30

© Author(s) 2024